Oxygen Atom Transfer Systems in Which the (μ-Oxo)dimolybdenum(V) Complex Formation Does Not Occur: Syntheses, Structures, and Reactivities of Monooxomolybdenum(IV) Benzenedithiolato Complexes as Models of Molybdenum Oxidoreductases

Hiroyuki Oku, Norikazu Ueyama, Mitsuru Kondo, and Akira Nakamura*

Department of Macromolecular Science, Faculty of Science, Osaka University, Toyonaka, Osaka 560, Japan

Received June 18, 1993®

Two monooxomolybdenum(IV) complexes with dithiolene-like benzenedithiolate ligands, $(NEt_4)_2[Mo^{IV}O(Ph_3Si\text{-}bdt)_2]$ (**1**) (Ph_3Si-bdt = 3-(triphenylsilyl)-1,2-benzenedithiolato) and $(NEt_4)_2[Mo^{IV}O(Ph_3Si\text{-}tdt)_2]$ (**2**) (Ph_3Si-tdt = 5-(triphenylsilyl)-3,4-toluenedithiolato), were synthesized as models of reduced state molybdenum oxidoreductase. The $MoOS_4$ cores of **1** and $(NEt_4)_2[Mo^{IV}O(tdt)_2]$ (**4**) (tdt = 3,4-toluenedithiolato) have a square pyramidal geometry similar to that of $(NEt_4)_2[Mo^{IV}O(bdt)_2]$ (**3**) (bdt = 1,2-benzenedithiolato) (Boyde et al., 1986). The substituent effect of the triphenylsilyl group was detected in UV/vis spectra and in electrochemical properties. In the UV/vis spectra the band energy and extinction coefficients of **1** and **2** (both with a Ph_3Si– group) are displaced to lower energy and slightly stronger (about 2,000 M^{-1} cm^{-1}) than **3** and **4**, respectively. The Mo(IV)/Mo(V) redox potential of **1** shows a negative shift (–0.03 V) compared with that of **3**. These differences are due to the direct or indirect effect of the electron donation from the phenyl group π orbital and the pπ orbital of sulfur atom. In contrast to **1**, **3**, and **4**, only the complex, **2**, that has the most bulky ligand, shows a quasi-reversible couple at +0.52 V (vs SCE) assignable to the Mo(V)/Mo(VI) redox process. The bulkiness of the ligand clearly contributes to the stabilization of the Mo(V)/Mo(VI) redox process of **2**. In the O atom transfer reaction of the monooxomolybdenum(IV) benzenedithiolate complex with Me_3NO, the corresponding dioxomolybdenum(VI) benzenedithiolate complex and Me_3N are formed quantitatively. This indicates the absence of (μ-oxo)dimolybdenum(V) complex formation in the present reaction controlled by the unique electronic properties and the strength of chelation of the dithiolato ligands.

Introduction

A number of studies have indicated that trimethylamine *N*-oxide (Me_3NO) reductase or dimethyl sulfoxide (DMSO) reductase from *Rhodopseudomonas sphaeroides* f.s. *denitrificans*,[1,2] *Escherichia coli*,[3,4] and other bacteria is a molybdoenzyme. The enzyme has been thought to be located at the end of a respiratory electron transfer chain linked to energy conservation and reduces the terminal electron acceptor, such as Me_3NO, DMSO, etc. The metal center is considered to be surrounded by many thiolate ligands[5] that include molybdoterpin (bactopterin)[6] such as those in the metal centers of other molybdenum oxidoreductases. The molybdopterin is a dithiolene ligand connecting phosphate and pterin derivatives. A resonance Raman study on Me_3NO/DMSO reductase from *R. sphaeroides* has suggested a chelating coordination of the dithiolate to Mo(IV) (reduced state) and Mo(VI) (oxidized state) center.[7] A similar type of coordination seems to be involved in the metal center of molybdenum oxidoreductases that contain molybdopterin.

The oxo accepting reaction (eq 1) with monooxomolybdenum(IV) complexes has been studied as models of reduced state active site.[8-10] Tertiary amine or aromatic amine *N*-oxides or *S*-oxides

$$(Mo^{IV}O)^{2+} + XO \rightarrow (Mo^{VI}O_2)^{2+} + X \qquad (1)$$

or nitrate was employed as an oxo donor. However, the following reaction (conproportionation to (μ-oxo)dimolybdenum(V) species) often makes the oxo transfer reaction more complicated.[11,12]

$$(Mo^{IV})^{2+} + (Mo^{VI}{=}O)^{2+} \rightleftharpoons (Mo^{V}{-}O{-}Mo^{V})^{4+} \qquad (2)$$

The (μ-oxo)dimolybdenum(V) species has been identified as the resting state of the oxo transfer reaction.

The formation of rather inert (μ-oxo)dimolybdenum(V) species generally proceeds by the presence of unreacted monooxomolybdenum(IV) and dioxomolybdenum(VI) species. These three species exist in an equilibrium,[13] and the position of the equilibrium has been considered to be regulated solely by the steric properties of ligands. Actually, sufficiently bulky tridentate or bidentate ligands prevents the reaction (eq 2).[14,15]

Two interesting points have been emphasized in the oxo transfer. First, if the monooxomolybdenum(IV) complex is to be used fully and efficiently as an reductant, *e.g.*, in the respiratory chain of bacteria which is essential for the life, one must avoid consuming half of it in the formation of inert (μ-oxo)dimolybdenum(V) species. Second, there is much evidence that molybdenum oxidoreductase actually employs a reaction like eq 1, where massive steric hindrance has been proposed to entirely suppress the dimerization (eq 2).

* Abstract published in *Advance ACS Abstracts*, December 15, 1993.

(1) Bastian, N. R.; Kay, C. J.; Barber, M. J.; Rajagopalan, K. V. *J. Biol. Chem.* **1991**, *266*, 45.
(2) Satoh, T.; Kurihara, F. N. *J. Biochem.* (*Tokyo*) **1987**, *102*, 191.
(3) Cammack, C.; Weiner, J. H. *Biochemistry* **1990**, *29*, 8410.
(4) Bilous, P. T.; Weiner, J. H. *J. Bacteriol.* **1985**, *163*, 396.
(5) Cramer, S. P.; Gray, H. B.; Rajagopalan, K. V. *J. Am. Chem. Soc.* **1979**, *101*, 2772. Tullius, T. D.; Kurtz, D. M., Jr.; Conradson, S. D.; Hodgson, K. O. *J. Am. Chem. Soc.* **1979**, *101*, 2776. Cramer, S. P.; Wahl, R.; Rajagopalan, K. V. *J. Am. Chem. Soc.* **1981**, *103*, 7721.
(6) Johnson, J. L.; Bastian, N. R.; Rajagopalan, K. V. *Proc. Natl. Acad. Sci. U.S.A.* **1990**, *87*, 3190. Bastian, N. R.; Kay, C. J.; Barber, M. J.; Rajagopalan, K. V. *J. Biol. Chem.* **1991**, *266*, 45.
(7) Subramanian, P.; Burgayer, S.; Richards, S.; Szalaki, V.; Spiro, T. G. *Inorg. Chem.* **1990**, *29*, 3849.
(8) Harlan, E. W.; Berg, J. M.; Holm, R. H. *J. Am. Chem. Soc.* **1986**, *108*, 6992.
(9) Craig, J. A.; Holm, R. H. *J. Am. Chem. Soc.* **1989**, *111*, 2111.
(10) Berg, J. M.; Holm, R. H. *J. Am. Chem. Soc.* **1985**, *107*, 925.
(11) Topich, J.; Lyon, J. T., III. *Inorg. Chem.* **1984**, *23*, 3202.
(12) Holm, R. H. *Coord. Chem. Rev.* **1990**, 183.
(13) Reynolds, M. S.; Berg, J. M.; Holm, R. H. *Inorg. Chem.* **1984**, *23*, 3057.
(14) Holm, R. H.; Berg, J. M. *Acc. Chem. Res.* **1986**, *19*, 363–370.
(15) Gheller, S. F.; Schultz, B. E.; Scott, M. J.; Holm, R. H. *J. Am. Chem. Soc.* **1992**, *114*, 6934. Schurtz, B. E.; Gheller, S. F.; Muetterties, M. C.; Scott, M. J.; Holm, R. H. *J. Am. Chem. Soc.* **1993**, *115*, 2714.

0020-1669/94/1333-0209$04.50/0

In addition to the steric factor, a recent report[15] indicates that the association of solvent on five-coordinated Mo(IV) species, $[Mo^{IV}O(t\text{-BuL-NS})_2]$ (*t*-BuL-NS = bis(4-*tert*-butylphenyl)-2-pyridylmethanethiolate) suppresses μ-oxo bridge formation in donor solvents such as acetonitrile, THF, and DMF.

Boyde *et al.* have reported the synthesis and crystal structure of $[Mo^{IV}O(bdt)_2]^{2-}$ (**3**) (bdt = 1,2-benzenedithiolato) as a model of the active site of the reduced form enzyme.[16] The bdt ligand has a dithiolene like chelate as a model of pterin cofactor. We have studied the catalytic activity of the above complex for the oxidation of benzoin by air or pyridine *N*-oxide.[17,18] During the catalytic cycle, the presence of $[Mo^{VI}O_2(bdt)_2]^{2-}$ (**7**) was suggested by spectroscopic methods.[19] A *cis*-dioxomolybdenum(VI) complex with two benzenedithiolate ligands was the first to be synthesized from the O atom transfer reaction between $[Mo^{IV}O(bdt)_2]^{2-}$ (**3**) and Me_3NO as a model for the active site of oxidized molybdenum oxidoreductase.[20]

Similar complexes, $[W^{IV}O(bdt)_2]^{2-}$ and $[W^{VI}O_2(bdt)_2]^{2-}$, were also synthesized by the O-atom transfer reaction as models of tungsten oxidoreductase.[21]

The dimerization reaction to μ-oxodimolybdenum(V) species, eq 2, has been blocked by the sterically bulky ligands. However, in the present case of the nonbulky 1,2-benzenedithiolato ligand, the reaction does not occur. An electronic property must be operative in our case.

Here we report the syntheses of model complexes for the reduced form of molybdenum oxidoreductases (especially, Me_3NO reductase) that have molybdenum(IV), terminal oxo, and substituted benzenedithiolato ligands as models of pterin cofacter, and also present their structure, properties, and reactivities, in particular with Me_3NO. To investigate the reaction mechanism between the monooxomolybdenum(IV) benzenedithiolato complex and Me_3NO, novel benzenedithiolato ligands with a bulky triphenylsilyl substituent were utilized for its characteristic steric and electronic properties.

Experimental Section

All operations were carried out under argon atmosphere. *N,N*-Dimethylformamide (DMF), diethyl ether, 1,2-dimethoxyethane (DME), acetonitrile, cyclohexane, and *N,N,N',N'*-tetramethylethylenediamine (TMEDA) were purified by distillation before use.

Materials. 1,2-Benzenedithiol ($bdtH_2$) was prepared by the reported procedure.[22] The 3,4-toluenedithiol ($tdtH_2$), triphenylsilyl chloride, and Me_3NO used were of commercial grade. $(NEt_4)_2[Mo^{IV}O(bdt)_2]$ (**3**) was prepared by the careful reduction of $(NEt_4)[Mo^{V}O(bdt)_2]$ with NEt_4BH_4 in acetonitrile.[24] Preparation of $(NEt_4)_2[Mo^{VI}O_2(Ph_3Si\text{-}bdt)_2]$ (**5**) and $(NEt_4)_2[Mo^{VI}O_2(tdt)_2]$ (**8**) is similar to the synthesis of **7**.[20]

3-(Triphenylsilyl)-1,2-benzenedithiol (Ph_3Si-$bdtH_2$). The title compound was prepared by a modified method reported for the synthesis of ortho-substituted thiophenol.[22] To 50 mL of cyclohexane was added 1,2-benzenedithiol (0.81 mL, 7.0 mmol) and *N,N,N',N'*-tetramethylethylenediamine at 0 °C, and a *n*-hexane solution (14.1 mL) of *n*-butyllithium (22.5 mmol) subsequently. The reaction mixture was stirred for 3 days, and triphenylsilyl chloride (4.20 g, 14.2 mmol) in THF (10 mL) was added to the solution at −78 °C. After being stirred for 2 h, the solution was allowed to stand at room temperature. To the solution was added 70 mL of a 10% HCl aqueous solution at 0 °C and 70 mL of diethyl ether. The ether layer was separated and washed with 100 mL of a 10% HCl aqueous solution three times and with 50 mL of a NaCl-saturated aqueous solution twice, successively. The solution was dried over anhydrous magnesium sulfate and concentrated under reduced pressure to give white powder which was recrystallized from diethyl ether. ^1H NMR (acetonitrile-d_3): δ 3.24 (s, 1H), 3.98 (br s, 1H), 6.99 (dd, 1H), 7.06 (t, 1H), 7.40 (br m, 9H). MS: *m/e* 399.2 ($[M\text{-}1]^+$).

5-(Triphenylsilyl)-3,4-toluenedithiol (Ph_3Si-$tdtH_2$). Ph_3Si-tdt was prepared by the same procedure as reported for Ph_3Si-$bdtH_2$. ^1H NMR (acetonitrile-d_3) δ 1.94 (s, 3H), 3.76 (s, 2H), 6.73 (dd, 1H), 7.26 (m, 7H), 7.34 (t, 3H), 7.42 (d, 6H). MS: *m/e* 412.0 ($[M - 2]^+$).

$(NEt_4)_2[Mo^{IV}O(Ph_3Si\text{-}bdt)_2]$ (1). To an acetonitrile solution (5 mL) of $(NEt_4)_2[Mo^{IV}O(p\text{-}S\text{-}C_6H_4Cl)_4]$ (**9**)[23] (0.17 g, 0.23 mmol) was added a DME solution (5 mL) of Ph_3Si-$bdtH_2$ (0.18 g, 0.46 mmol). The solution turned to a red-brownish color immediately, and then yellow microcrystals formed. The precipitates were collected with filtration and recrystallized from acetonitrile–diethyl ether. Yield, 150 mg (67%). ^1H NMR (acetonitrile-d_3): δ 6.55 (dd, 2H), 6.60 (t, 2H), 7.23 (t, 6H), 7.31 (m, 13H), 7.55 (d, 12H). Anal. Calcd for $C_{64}H_{76}N_2O_2S_4Si_2Mo$: C, 65.72; H, 6.55; N, 2.39. Found: C, 64.71; H, 6.45; N, 2.32. FAB-MS (negative): *m/e* 911 ($[M + 1]^-$).

$(NEt_4)_2[Mo^{IV}O(Ph_3Si\text{-}tdt)_2]$ (2). To an acetonitrile solution (15 mL) of **9** (0.25 g, 0.34 mmol), was added a DME solution (5 mL) of Ph_3Si-$tdtH_2$ (0.47 g, 0.68 mmol), and the mixture was kept under stirring for 10 min. The formed yellow crystals were filtered and recrystallized from acetonitrile–diethyl ether. Yield: 179 mg (44%). Mp: 150 °C dec. ^1H NMR (acetonitrile-d_3): δ 1.94 (t, 6H), 6.28 (q, 2H), 7.12 (t, 12H), 7.20 (t, 6H), 7.35 (d, 12H), 7.38 (q, 2H). Anal. Calcd for $C_{66}H_{80}N_2OS_4Mo$: C, 66.18; H, 6.73; N, 2.34. Found: C, 64.59; H, 6.83; N, 6.53. FAB-MS (negative): *m/e* 938 ($[M]^-$).

$(NEt_4)_2[Mo^{IV}O(tdt)_2]$ (4). To an acetonitrile solution (15 mL) of **9** (0.51 g, 0.67 mmol) was added a DME solution (60 mL) of $tdtH_2$ (0.23 mL, 1.3 mmol) at room temperature, and it was stirred for 10 min. The obtained yellow crystals were collected with filtration and recrystallized from acetonitrile–diethyl ether. Yield: 140 mg (53%). ^1H NMR (acetonitrile-d_3): δ 7.35 (dd, 2H), 7.33 (dq, 2H), 6.54 (dq, 2H), 2.18 (s, 6H). Anal. Calcd for $C_{30}H_{52}N_2OS_4Mo$: C, 52.92; H, 7.70; N, 4.11. Found: C, 52.69; H, 7.64; N, 4.63.

$(NEt_4)_2[Mo^{VI}O_2(Ph_3Si\text{-}tdt)_2]$ (6). To a DMF solution (5 mL) of $(NEt_4)_2[Mo^{IV}O(Ph_3Si\text{-}tdt)_2]$ (53 mg, 0.044 mmol) was added to a DMF solution (1 mL) of trimethylamine *N*-oxide (3 mg, 0.13 mmol) at room temperature. The solution became red-brown from a pale yellow. Red-brownish microcrystals were obtained with addition of 15 mL of diethyl ether to the DMF solution. Yield: 40 mg (70%). Mp: 194 °C dec. ^1H NMR (DMSO-d_6): δ 6.27 (dd, 2H), 6.95 (dd, 2H), 7.16 (t, 12H), 7.25 (t, 12H), 7.37 (t, 6H), 7.49 (d, 12H). Anal. Calcd for $C_{66}H_{80}N_2O_2Si_2S_4Mo$: C, 65.31; H, 6.64; N, 2.31. Found: C, 60.22; H, 6.34; N, 2.30. FAB-MS (negative): *m/e* 952 ($[M - 2]^{2-}$).

Physical Measurements. The absorption spectra were recorded on a Jasco Ubest-30 using a 1 mm cell under argon atmosphere. The extinction coefficients were given in M^{-1} cm^{-1}. Raman and IR spectra were taken on a Jasco R-800 spectrophotometer with a 514.5-nm excitation line and on a Jasco DS-402G spectrophotometer, respectively. The cyclic voltammograms were measured on a Yanaco P-1100 with a three-electrode system consisting of a glassy-carbon working electrode, a platinum-wire auxiliary electrode, and a saturated calomel compartment. The sample concentrations were 1 mM in DMF, and a solution of tetra-*n*-butylammonium perchlorate (0.1 M) was employed as a supporting electrolyte. Mass spectra were recorded on a JEOL JMS-SX102 mass spectrometer. DMF solutions of samples (10 nmol/2 μL) for the FAB-MS spectra and the matrix (magic bullet, 2 μL) were mixed on a stainless steel probe tip and then subjected to bombardment with xenon atoms.

Kinetic Measurements. Reaction systems containing the monooxomolybdenum(IV) complex and Me_3NO systems were monitored spectrophotometrically in the region 250–900 nm. A typical measurement was carried out using a 1-mm UV cell containing a solution of monooxomolybdenum(IV) benzenedithiolate complex (1 mM) at 27 °C. After thermal equilibrium, a Me_3NO solution (ca. 100 mM, also at 27 °C) was injected through a silicone rubber cap, and the cell contents were quickly mixed by shaking. The time dependence of the absorbance for dioxomolybdenum(VI) was measured every 2.5 min. All calculations for the data analysis were performed at 430 and 534 nm (O and S → Mo^{VI} charge transfer band).

The temperature dependence of the oxidation reaction at low temperature, 263, 253 and 243 K, was monitored using a 400-MHz ^1H

(16) Boyde, S.; Ellis, S. R.; Garner, C. D.; Clegg, W. *J. Chem. Soc., Chem. Commun.* **1986**, 1541.
(17) Ueyama, N.; Kamabuchi, K.; Nakamura, A. *J. Chem. Soc., Dalton Trans.* **1985**, 635.
(18) Ueyama, N.; Kamabuchi, K.; Nakamura, A. *J. Chem. Soc., Dalton Trans.* **1990**, 387.
(19) Ueyama, N.; Yoshinaga, N.; Okamura, T.; Zaima, H.; Nakamura, A. *J. Mol. Cata.* **1991**, *64*, 247–256.
(20) Yoshinaga, N.; Ueyama, N.; Okamura, T.; Nakamura, A. *Chem. Lett.* **1990**, 1655.
(21) Ueyama, N.; Oku, H.; Nakamura, A. *J. Am. Chem. Soc.* **1992**, *114*, 7311.
(22) Figuly, G. D.; Loop, C. K.; Martin, J. C. *J. Am. Chem. Soc.* **111**, 654 (1989).
(23) Kondo, M.; Ueyama, N.; Nakamura, A. *Bull. Chem. Soc. Jpn.*, in press.
(24) Ueyama, N.; Yoshinaga, N.; Okamura, T.; Zaima, T.; Nakamura, A. *J. Mol. Catal.* **1989**, *55*, 284.

Table 1. Crystal and Refinement Data for $(NEt_4)_2[Mo^{IV}O(Ph_3Si\text{-}bdt)_2]\cdot DMF$ (**1**·DMF) and $(NEt_4)_2[Mo^{IV}O(tdt)_2]$ (**4**)

	1·DMF	4
chemical formula	$C_{67}H_{83}ON_3MoS_4Si_2$	$C_{30}H_{52}ON_2MoS_4$
mw	1242.76	680.93
cryst syst	orthorhombic	monoclinic
color	orange	orange
cryst shape	plate	prism
space group	*Pbca* (No. 61)	$P2_1$ (No. 4)
a, Å	34.373(8)	9.244(4)
b, Å	25.246(6)	13.929(3)
c, Å	15.136(5)	13.554(3)
β, deg		97.88(2)
V, Å^3	13134(5)	1728.7
Z	8	2
d_{calc}, g cm^{-3}	1.257	1.308
radiation	Mo Kα	Mo Kα
μ(Mo Kα), cm^{-1}	3.95	6.26
temp, °C	23	23
scan speed, deg min^{-1}	8	8
2θ range, deg	6–55	6–60
octants	$+h,+k,+l$	$+h,+k,\pm l$
no. of reflcns (tot.)	16 356	5576
(unique)	16 356	5286 (R_{int} = 0.022)
no. of data used ($I_o > 3\sigma(I)$)	6054	3582
R	0.055	0.045
R_w	0.058	0.055

NMR spectrometer (JEOL GSX-400) with measurements of the ^{1}H signals of Me_3N and the benzenedithiolate phenyl protons of dioxomolybdenum(VI) complexes. A solution of Me_3NO (10 mM DMF-d_7) in a 5-mm NMR gastight tube containing a monooxomolybdenum(IV) benzenedithiolate complex solution (1 mM) in DMF-d_7 was prepared under an argon atmosphere, and the contents were quickly mixed by shaking at 27 °C and cooled at −78 °C. The ^{1}H NMR spectra were taken every 30 min.

Crystallographic Data Collections and Data Reduction. Orange crystals of **1**·DMF and **4** were mounted in a glass capillary under argon atmosphere. All measurements were made on a Rigaku AFC-5R diffractometer with graphite-monochromated Mo Kα radiation and a 12-kW rotating anode generator. Cell constants and an orientation matrix for data collection, obtained from a least-squares refinement using the setting angle of 25 carefully centered reflections in the range $29.7° < 2\theta < 30.0°$ corresponded to a orthorhombic cell for **1**·DMF and a monoclinic cell for **4**, with dimensions listed in Table 1. On the basis of the systematic absences, the successful solutions, and refinement of the structures, the space groups were determined to be *Pbca* for **1**·DMF and $P2_1$ for **4**. The data were collected at 23 °C using the ω scan technique to a maximum 2θ value of 55.1° for **1**·DMF and 60.1° for **4**.

Of the 16 356 and 5576 reflections collected for **1**·DMF and **4**, respectively, which were collected, 16 356 and 5286 for **1**·DMF and **4**, respectively, were unique. The intensities of three representative reflections, measured after every 100 reflections, were shown to be without any significant change. The linear absorption coefficient for Mo Kα is 3.9 cm^{-1} in **1**·DMF and 6.3 cm^{-1} in **4**. An empirical absorption correction, based on azimuthal scans of three reflections, was applied which resulted in transmission factors ranging from 0.89 to 1.00 and 0.93 to 1.00 for **1**·DMF and **4**, respectively. The data were corrected for Lorentz and polarization effects.

Structure Solution and Refinement. The positions of Mo atoms were determined by the heavy-atom method. Other non-hydrogen atom sites were located on subsequent Fourier syntheses following least-squares refinements of the Mo atom. The non-hydrogen atoms were refined anisotropically. Hydrogen atom coordinates were included at idealized positions with a assumed C–H distance of 1.08 Å, and the hydrogen atoms were given with the same temperature facter as that of the carbon atoms to which they were bonded. The final cycles of least-squares refinement were based on 6069 for **1**·DMF and 3582 for **4** observed reflections ($I > 3.00\sigma(I)$) and 790 for **1**·DMF and 595 for **4** variable parameters and converged with R = 0.055 and R_w = 0.058 for **1**·DMF and R = 0.045 and R_w = 0.055 for **4**. The factors are defined as $R = \sum(|F_o| - |F_c|)/\sum|F_o|$ and $R_w = [\sum w(|F_o| - |F_c|)^2/\sum w|F_o|^2]^{1/2}$.

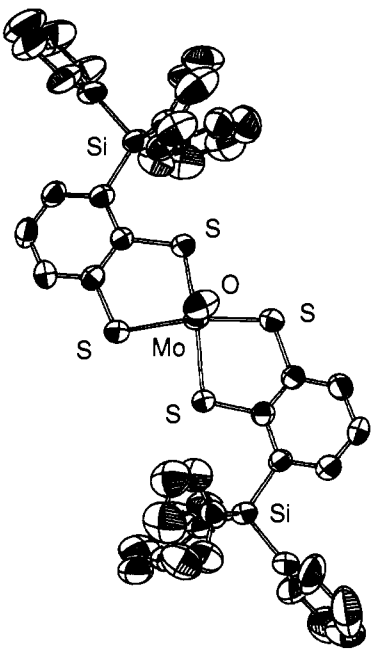

Figure 1. ORTEP drawing of the anion part of $(NEt_4)_2[Mo^{IV}O(Ph_3Si\text{-}bdt)_2]\cdot DMF$ (**1**·DMF). The 50% probability ellipsoids are shown.

Neutral atom scattering factors were taken from ref 25. Anomalous dispersion effects were included in F_{calc}; the values for $\Delta f'$ and $\Delta f''$ were taken from ref 25. All calculations were performed using the TEXAN crystallographic software package of the Molecular Structure Corp.

Results and Discussion

Synthetic Studies. The bulky benzene-1,2-dithiols $Ph_3Si\text{-}bdtH_2$ and $Ph_3Si\text{-}tdtH_2$, were prepared by directed ortho-lithiation[22] of the corresponding dithiols, $tdtH_2$ and $bdtH_2$, respectively, with *n*-butyllithium. $TdtH_2$ reacted with *n*-butyllithium only at the 5-position. The lithiation product at the 2-position was not observed. **1**, **2**, and **4** were prepared by the ligand exchange reaction of the monodentate thiolato complex **9** with the corresponding dithiols in DME. **4** was synthesized by a different method from that reported for $K_2[Mo^{IV}O(tdt)_2]$ by Mitchel *et al.*[26] The reaction of **9** with 3 equiv of $tdtH_2$ yields the tris(dithiolato)molybdenum(IV) complex $(NEt_4)_2[Mo^{IV}(tdt)_3]$.[27] The monooxo complex, **4**, was not found. On the contrary, in the case of bulky ligands, e.g., $Ph_3Si\text{-}tdtH_2$ and $Ph_3Si\text{-}bdtH_2$, the tris complexes, $(NEt_4)_2[Mo^{IV}(Ph_3Si\text{-}tdt)_3]$ and $(NEt_4)_2[Mo^{IV}(Ph_3Si\text{-}bdt)_3]$, were not produced. Utilizing the bulky benzenedithiolate, a third coordination of the dithiolate to bis(benzenedithiolato)monooxomolybdenum(IV) complex was blocked in the ligand-exchange reaction. Similarly, bulky benzenedithiolate also prevents the formation of the tris(benzenedithiolato)molybdenum(V) complex $(NEt_4)[M^V(Ph_3Si\text{-}bdt)_3]$ from $(NEt_4)[M^VO(Ph_3Si\text{-}bdt)_2]$ (M = Mo and W), which results from $(NEt_4)[M^VO(SPh)_4]$ (M = Mo and W) with 3 equiv of $Ph_3Si\text{-}bdtH_2$.

Crystal Structure of 1·DMF. The anion structure of **1**·DMF is shown in Figure 1 and the selected structural parameters are listed in Table 2. In an unit cell eight molecules exist as four enantiomeric pairs. Each pair has mirror planes or inversion centers between the two molecules. The ligands are in a mutually trans configuration. In this structure, Et_4N^+ cations were finely resolved. Two cations in the asymmetric unit are well separated from two anions.

The $MoOS_4$ core of $[Mo^{IV}O(Ph_3Si\text{-}bdt)_2]^{2-}$ has an approximately square pyramidal geometry (C_{2v} symmetry) with the

(25) Cromer, D. T. and Waber, J. T. *International Tables for X-ray Crystallography*; The Kynoch Press: Birmingham, England, 1974; Vol. IV, Table 2.2A and Table 2.3.1.
(26) Mitchell, P. C. H.; Pygall, C. F. *Inorg. Chim. Acta* **1979**, *33*, L109.
(27) Rice, C. A.; Spence, J. T. *Inorg. Chem.* **1980**, *19*, 2845.

Table 2. Comparison of $MoOS_4C_4$ dimensions (Å, deg) for $(NEt_4)_2[Mo^{IV}O(Ph_3Si\text{-}bdt)_2]\cdot DMF$ (**1**·DMF), $(NEt_4)_2[Mo^{IV}O(bdt)_2]$ (**3**), and $(NEt_4)_2[Mo^{IV}O(tdt)_2]$ (**4**)[a]

	1·DMF	4: anion a and anion b	3: anion I and anion II[16]
Mo=O	1.677(4)	1.666(5)	1.700(9) 1.694
Mo—S (mean)	2.387(16)	2.384(3)	2.388(5)
range	2.368(2)–2.404(2)	2.371(3)–2.536(4) 2.383(7) 2.296(7)–2.461(7)	2.384(2)–2.391(2) 2.383(6) 2.379–2.387
S—C (mean)	1.763(6)	1.75(1)	1.766(0)
range	1.757(6)–1.771(6)	1.50(1)–1.93(1) 1.81(2) 1.40(2)–2.03(2)	1.766(6)–1.766(6) 1.771(9) 1.755–1.768
∠(Mo–S–C) (mean)	107.2(4)	106.3(69)	107.6(2)
range	106.7(2)–107.6(2)	114.5(5)–100.3(3) 108.0(126) 96.9(5)–125.5(8)	107.5–107.8 107.4(0) 107.4–107.4
∠(O–Mo–S) (mean)	108.6(14)	107.5(6)	108.2(17)
range	106.7(2)–110.0(2)	106.6(2)–108.0(2) 108.0(8) 107.0(3)–109.0(3)	106.9–109.4 108.3(6) 107.9–108.7
displacement of Mo atom from S_4 plane	0.76(4)	0.71(1) 0.734(1)	0.745(1)

[a] The number in the parentheses represents the individual standard deviation or the standard deviations from the mean, σ. $\sigma = (\sum^{N}_{i=1}(x_i - x_{mean})^2/N(N-1))^{1/2}$.

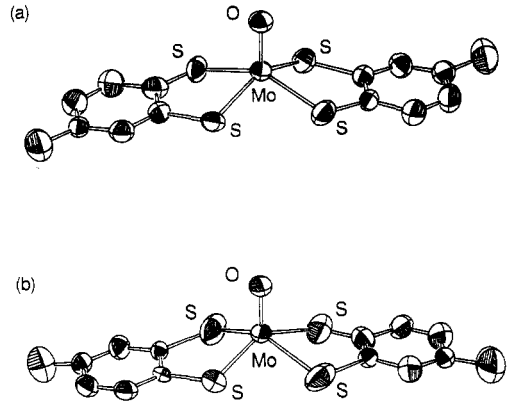

Figure 2. ORTEP drawings of the anion part of $(NEt_4)_2[Mo^{IV}O(tdt)_2]$ (**4**) (a, b). The 50% probability ellipsoids are shown.

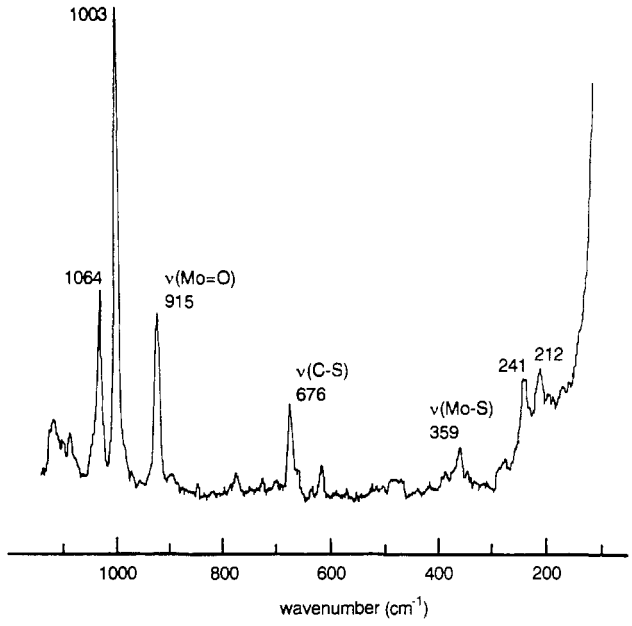

Figure 3. Raman spectrum of $(NEt_4)_2[Mo^{IV}O(Ph_3Si\text{-}bdt)_2]\cdot DMF$ (**1**·DMF). (514.5 nm excitation.) A single crystal was used.

oxygen atom at the apex and the molybdenum atom raised slightly above the basal (S_4) plane. The selected bond distances and bond angles of **1**·DMF are listed in Table 2. The mean parameters of $MoOS_4C_4$ moiety of **1**·DMF are similar to those of **3**.[16] However, each parameter of the moiety is different from each parameter in **3**. The values range as follows: Mo=O distance, 1.677(4) Å; Mo–S distance, 2.368(2)–2.404(2) Å; S–C distance, 1.757(6)–1.771(6) Å; Mo–S–C angle, 106.7(2)–107.6(2)°.

All phenyl rings of the triphenylsilyl group are located to the outside for more than 3.5 Å from the S atom (S $p\pi$ orbital). Any significant substituent effect of the triphenylsilyl group was not observed in the crystal structure. In other spectroscopic features, interaction between the S $p\pi$ orbital and the π orbital of the phenyl group was observed and will be discussed later.

Crystal Structure of 4. The anion structure of **4** is shown in Figure 2 and selected structural parameters are listed in Table 2. In an asymmetric unit, enantiomeric anions are located on the same position. Absolute configurations are not determined. Two enantiomers share Mo and O atoms and show the left and right hands along a 2-fold rotation axis formed by the ligands. The ratios of occupancies are 0.6 and 0.4 for anions a and b. (From the occupancies, the trans configuration of ligands was determined.)

The $MoOS_4$ core of **4** has an approximately square pyramidal geometry (C_{2v} symmetry) with the oxygen atom at the apex and the molybdenum atom raised slightly above the basal S_4 plane (0.71–0.73 Å). The mean parameters of $MoOS_4C_4$ moiety of **4** are also similar to **3**. Because of the disorder problem, each dimension shows unusual values except for Mo=O bond length (1.666(5) Å).

UV/vis Absorption Spectra of 1–4. In Table 3, the UV/vis absorption maxima are shown. As shown in Figure 4, a strong absorption bond and two or one weak absorption bands are observed at about 360 and 440 nm, respectively, for **1**–**4** in DMF. The extinction coefficients for **1** and **2** are 13 000 M^{-1} cm^{-1} (at 359 nm) and 15 000 M^{-1} cm^{-1} (at 363 nm), respectively. These magnitudes are stronger than 12 000 M^{-1} cm^{-1} (at 328 nm) and 11 000 M^{-1} cm^{-1} (at 331 nm) for **3** and **4**, respectively. The band energies for **1** and **2** at about 360 nm are displaced to lower energy than those for **3** and **4** (at 330 nm). These differences are due to the electron-donating effect of the triphenylsilyl group (Ph_3Si– group) through the benzene ring, which serves as an

Table 3. Raman (IR) Bands of ν(Mo=O) and ν(Mo—S) and UV/Vis Absorption Maxima and Redox Potentials of $(NEt_4)_2[Mo^{IV}O(Ph_3Si\text{-}bdt)_2]$ (**1**), $(NEt_4)_2[Mo^{IV}O(Ph_3Si\text{-}tdt)_2]$ (**2**), $(NEt_4)_2[Mo^{IV}O(bdt)_2]$ (**3**), and $(NEt_4)_2[Mo^{IV}O(tdt)_2]$ (**4**)

	raman (IR) band in the solid state, cm^{-1}			redox potential in DMF V vs SCE		
complex	ν(Mo=O)	ν(Mo—S)	UV/vis abs in DMF λ_{max}, nm (ϵ, M^{-1} cm^{-1})	Mo^{IV}/Mo^{V}	Mo^{V}/Mo^{VI}	E_a / E_c
1	915 (910)	365	359 (13000)	–0.41		...
			445 (1300)			+0.62
2	900 (901)	360	363 (15000)	–0.45		...
			447 (1600)			+0.65
3	902 (905)	356	328 (12000)	–0.38		...
			385 (980)			+0.65
			452 (470)			
4	904 (905)	357	331 (11000)	–0.46	+0.52	+0.38
			380 (700)			+0.66
			454 (370)			

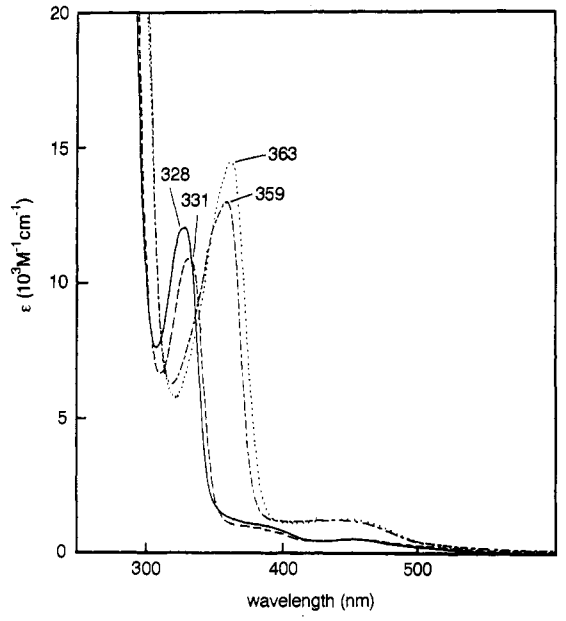

Figure 4. UV/vis spectra of $(NEt_4)_2[Mo^{IV}O(Ph_3Si\text{-}bdt)_2]$ (**1**) (···), $(NEt_4)_2[Mo^{IV}O(Ph_3Si\text{-}tdt)_2]$ (**2**) (– · –), $(NEt_4)_2[Mo^{IV}O(bdt)_2]$ (**3**) (—) and $(NEt_4)_2[Mo^{IV}O(tdt)_2]$ (**4**) (– –) in DMF.

electron buffer with a conjugation between S pπ and phenyl π orbitals. Similar conjugation is observed in the model systems of iron–sulfate proteins[28] in which the π–π interaction could provide a channel for electron transfer. The substituent effect shows the tendency Ph_3Si-bdt (**1**) < Ph_3Si-tdt (**2**) or bdt (**3**) < tdt (**4**) and reflects the difference of LMCT bands[29] (Δ(**1** – **2**) = –4 nm and Δ(**3** – **4**) = –3 nm). An absorption maximum with comparable energy and weaker intensity has been reported to be observed at 350 nm (ϵ = 5300 M^{-1} cm^{-1}) in reduced DMSO reductase[1] from *R. sphaeroides* f.s. *denitrificans* and has been assigned to the molybdenum chromophore because the molybdenum center is only one chromophore in this enzyme, different from other molybdenum oxidoreductases.

Electrochemical Properties. The cyclic voltammograms of **2** in DMF are shown in Figure 5. The redox potentials of **1**–**4** are shown in Table 3. **1** and **2** exhibit quasi-reversible redox couples at –0.41 and –0.46 V (vs SCE), respectively. These couples are assignable to the Mo(IV)/Mo(V) couples. A comparison of $E_{1/2}$ values between **1** and **2** and between **3** and **4** shows that the introduction of the substituent methyl group changes the $E_{1/2}$ value by –0.04 V (Δ(**1** – **2**)) and –0.07 V (Δ(**3** – **4**)) (vs SCE). The observed shift is ascribed to elevation of the occupied Mo 4d energy level due to the electron donating methyl group.

The above rationale explains also the blue shifts of the LMCT bands between **1** and **2** and between **3** and **4**. The substituent effect of Ph_3Si– group is different in each complex. A comparison between **1** and **3** shows the result of a negative shift by –0.03 V, and no difference was observed between **2** and **4**. Also these electronic effects contribute to the slight redox potential change through the conjugation between the π orbital of phenyl group and the pπ orbital of sulfur atom.

In contrast to **1**, **3** and **4**, only the complex, **2**, that has the most bulky ligand, shows a quasi-reversible couple at +0.52 V (vs SCE). Other complexes, **1**, **3**, and **4** show no clear reductive peaks in the range from +0.35 to +0.45 V (vs SCE), and only a clear oxidative peak appears at about +0.6 V (vs SCE). These oxidative and reductive peaks are assignable to the Mo(V)/Mo(VI) couples. The stable Mo(V)/Mo(VI) couple has been reported only at low temperature for the monooxomolybdenum(V) thiophenolate complex.[30] The bulkiness of the ligand clearly contributes to the stabilization of the Mo(V)/Mo(VI) redox process of **2**.

Raman and IR Spectra. In Table 3 and Figure 3, Raman(IR) bands of ν(Mo=O) and ν(Mo—S) are shown. Monooxomolybdenum(IV) benzenedithiolate complexes **1**–**4** exhibit strong Raman (IR) bands at 915 (910), 902 (903), 902 (905) and 904 (905) cm^{-1}, respectively. These bands are assignable to the vibrations related with Mo=O bonds.[16] Furthermore, a relatively weak Raman band is observed at 365, 360, 356, and 357 cm^{-1} for **1**–**4**, respectively. These bands are associated with the vibrations of Mo–S bonds.[16] The trend of the difference (–0.020 Å) in Mo=O bond length between **1**·DMF and **3** is consistent with the wavenumber difference (Δ(**1**·DMF – **3**) = –13 (–5) cm^{-1} in Raman (IR), respectively) of the ν(Mo=O) band. However, the similarity of the Mo–S bond lengths between **1**·DMF and **3** is not in line with the difference (Δ(**1**·DMF – **3**) = –9 cm^{-1}) in the shift of these ν(Mo–S) bands.

Disagreement in the trends between Mo–S bond length and the Raman band frequencies comes from the different conformation of the MoS_2C_2 chelate ring (Mo–S–C–C dihedral angle). Angular dependences of the frequencies associated with metal–sulfur bond stretching have already been observed or calculated for $[Fe_2S_2(SR)_4]^{2-}$ and $[Fe(SR)_4]^{2-}$ complexes.[31] Thus, the Fe–S stretching mode depends on the Fe–S–C–C dihedral angle. For organic disulfides,[32] the frequencies of S–S stretching mode are influenced by the S–S–C–C dihedral angle. When the Mo–S–C–C dihedral angle is 0°, then the S–C–C bend and the Mo–S stretch are in the same plane and coupling between them is maximal, whereas the coupling is minimized when the angle is 90°. As the Mo–S–C–C dihedral angle decreases, from 15°

(28) Sun, W. Y.; Ueyama, N.; Nakamura, A. *Inorg. Chem.* **1993**, *32*, 1095.
(29) Lever, A. B. P. *Inorganic Electronic Spectroscopy*; Elsevier: Amsterdam, 1968; p 224.
(30) Bradbury, J. R.; Masters, A. F.; McDonell, A. C.; Brunette, A. A.; Bond, A. M.; Wedd, A. G. *J. Am. Chem. Soc.* **1981**, *103*, 1959.
(31) Han, S.; Czernuszewicz, R. S.; Spiro, T. G. *J. Am. Chem. Soc.* **1989**, *111*, 3496. Yachandra, V. K.; Hare, J.; Moura, I.; Spiro, T. G. *J. Am. Chem. Soc.* **1983**, *105*, 6455.
(32) Sugeta, H.; Go, A.; Miyazawa, T. *Chem. Lett.* **1972**, 83.

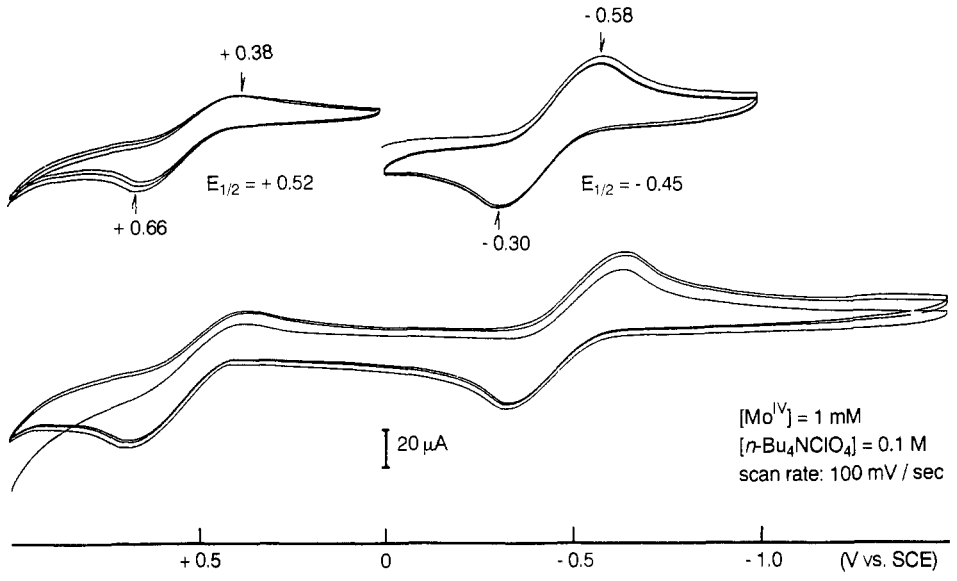

Figure 5. Cyclic voltammograms of $(NEt_4)_2[Mo^{IV}O(Ph_3Si\text{-}tdt)_2]$ (**2**) in DMF.

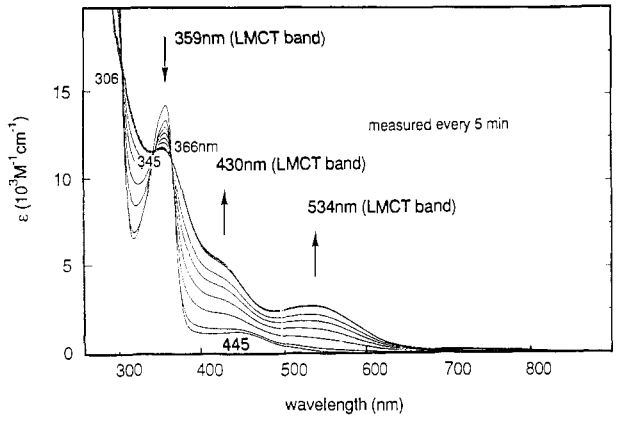

Figure 6. UV/vis spectral change (measured every 5 min) in the oxidation of $(NEt_4)_2[Mo^{IV}O(Ph_3Si\text{-}bdt)_2]$ (**1**) with Me_3NO. Reaction conditions: [Mo] = 1 mM, [Me_3NO] = 2 mM, in DMF at 27 °C.

(mean value in **1**) toward 9.8° (mean value in **3**), the band associated with ν(Mo–S) decreases from 365 cm^{-1} (**1**) toward 356 cm^{-1} (**3**) reflecting the expected influence from the MoS_2C_2 chelate ring conformation, although the bending band related with δ(S–C–C) has not been assigned.

Reaction with Trimethylamine *N*-Oxide. The spectroscopic course of reaction between **1** and Me_3NO at the ratio $[\mathbf{1}]_0$:$[Me_3NO]_0$ = 1:2 is presented in Figure 6. As expected for the spectrum of the Mo(IV) complex, e.g., **1**, the maxima at 359 nm diminishes with time, showing tight isosbestic points at 306, 345, and 366 nm. The final spectrum, with λ_{max} = 356, 430, and 534 nm, demonstrates the quantitative formation of the Mo(VI) complex $(NEt_4)_2[Mo^{VI}O_2(Ph_3Si\text{-}bdt)_2]$ (**5**).[33] A (μ-oxo)dimolybdenum(V) complex was not formed. Thus, we concluded the reactions to be clean and to follow eq 3. Also in each case of **2**–**4**, Me_3NO

$$[Mo^{IV}O(bdt)_2]^{2-} + Me_3NO \rightarrow [Mo^{VI}O_2(bdt)_2]^{2-} + Me_3N \quad (3)$$

was reduced and the corresponding dioxomolybdenum(VI) complexes $(NEt_4)_2[Mo^{VI}O_2(Ph_3Si\text{-}tdt)_2]$ (**6**), $(NEt_4)_2[Mo^{VI}O_2(bdt)_2]$ (**7**), and $(NEt_4)_2[Mo^{VI}O_2(tdt)_2]$ (**8**) formed.

Time conversion curves for **1** and **3** from UV/vis spectra are shown in Figure 7 and were analyzed by pseudo-first-order kinetics. The obtained rate constants are listed in Figure 7 and are presented by the dependences on Me_3NO concentration in Figure 8. The time conversion curve of **3** ([Me_3NO] = 2 mM) was bent at 12 min. The results suggest the reduction of Me_3NO in two steps. In the case of **1**, the bending was observed only under the stoichiometric condition. As shown in Figure 8, the system of **1** exhibits saturation kinetics at sufficiently high substrate concentration ([Me_3NO] > 6 mM). Under these conditions, the reaction proceeds with first-order kinetics for the Mo(IV) complex **1** and the rate constant (k_{obs} = 2.5 × 10^{-3} s^{-1}) is independent of Me_3NO concentration. In contrast to the case of **1**, no saturation was observed for **3**. Thus, the bulkiness of the Ph_3Si– group in **1** significantly decreases the rate constant.

A proposed reaction pathway is shown in Figure 9. The reversible coordination of Me_3NO to **1** gives a possible intermediate complex as shown in Figure 9. By the trans–cis rearrangement among Ph_3Si-bdt ligands and oxo ligands, the intermediate complex gives an intramolecular O atom transfer product, the *cis*-dioxomolybdenum(VI) complex **5**.

The rate constant for **3** (k_{obs} = 9.5 × 10^{-4} s^{-1}) at low concentration of Me_3NO ([Me_3NO] = 2 mM) is larger than that of **1** (k_{obs} = 3.9 × 10^{-4} s^{-1}) as shown in Figures 7 and 8. This indicates that the less polar or low dielectric space made from the bulky Ph_3Si– group enhances the rate-determining coordination of Me_3NO to the Mo(IV) center and stabilizes the associative intermediate at that concentration of Me_3NO. Similar strengthening of electrostatic interaction is observed in the model systems of iron–sulfur proteins in which an aromatic group stabilizes the Fe–S bond of the model complexes against to air and water,[34] and the nonpolar solvent or hydrophobic side chain of amino acid residues supports the formation of NH---S hydrogen bond.[35]

Comparison of rate constants for **1**–**4** in 10-fold excess of Me_3NO is summarized in Table 4. If the rate-determining cleavage of the N–O bond and the release of Me_3N from the reaction intermediate (as shown in Figure 9) are involved, electron-donating substituent (methyl group) on the thiolato ligands is expected to labilize the N–O bond and accelerate the reaction rate. The presence of similar internal electron donors has been demonstrated in the oxidation reaction by heme enzymes[36] and model systems[37]

(33) λ_{max} = 356 nm (ϵ = 13 000 cm^{-1}), 430 nm (sh, ϵ = 6100 cm^{-1}) and 534 nm (ϵ = 3400 cm^{-1}).

(34) Sun, W. Y.; Ueyama, N.; Nakamura, A. *Tetrahedron* **1992**, *48*, 1557. Sun, W. Y. Ph.D. Thesis, Osaka University, 1993.
(35) Sun, W. Y.; Ueyama, N.; Nakamura, A. *Inorg. Chem.* **1991**, *30*, 4026. Sun, W. Y.; Ueyama, N.; Nakamura, A. *Inorg. Chem.* **1992**, *31*, 4053.
(36) Dawson, J. H.; Holm, R. H.; Trundell, J. R.; Barth, G.; Linder, R. E.; Bunnenberg, E.; Djerassi, C. *J. Am. Chem. Soc.* **1976**, *98*, 3707. Poulos, T. L.; Kraut, J. *J. Biol. Chem.* **1980**, *255*, 8199. Dawson, J. H. *Science* **1988**, *240*, 433.

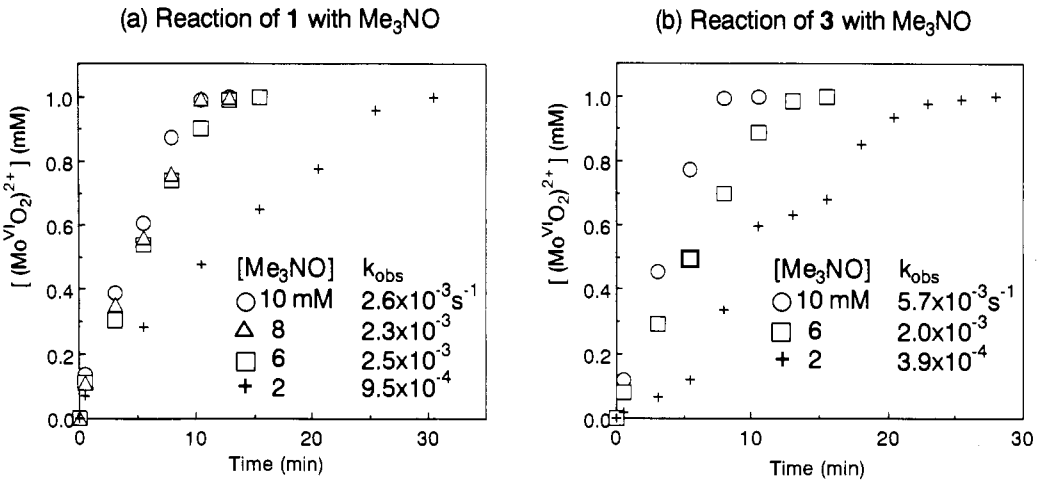

Figure 7. UV/vis time conversion curve of the reaction of $(NEt_4)_2[Mo^{IV}O(Ph_3Si\text{-}bdt)_2]$ (**1**) and $(NEt_4)_2[Mo^{IV}O(bdt)_2]$ (**3**) with Me_3NO in DMF at 27 °C ([Mo] = 1 mM).

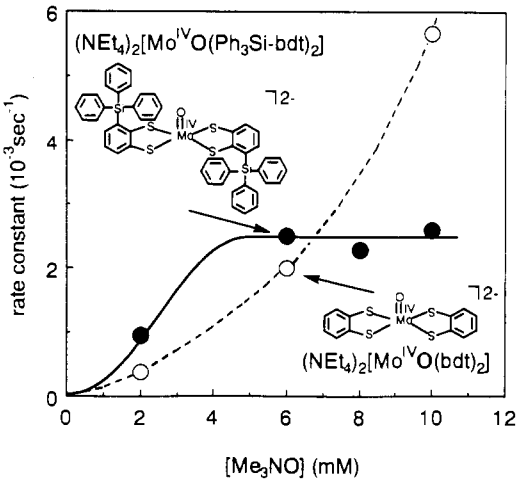

Figure 8. Rate constants of the reaction between $(NEt_4)_2[Mo^{IV}O(Ph_3Si\text{-}bdt)_2]$ (**1**) (—) and $(NEt_4)_2[Mo^{IV}O(bdt)_2]$ (**3**) (- - -) (1 mM) with increasing concentration of Me_3NO (2–10 mM) in DMF at 27 °C. Data were analyzed by pseudo-first-order kinetics, $d[Mo^{IV}]/dt = -k_{obs}[Mo^{IV}]$.

Table 4. Comparison of Rate Constants[38] in the Oxidation of $(NEt_4)_2[Mo^{IV}O(Ph_3Si\text{-}bdt)_2]$ (**1**), $(NEt_4)_2[Mo^{IV}O(Ph_3Si\text{-}tdt)_2]$ (**2**), $(NEt_4)_2[Mo^{IV}O(bdt)_2]$ (**3**), and $(NEt_4)_2[Mo^{IV}O(tdt)_2]$ (**4**) with Me_3NO[a]

complex	k_{obs}, 10^{-3} s^{-1}
1	2.6 ± 0.5
2	2.0 ± 0.1
3	5.7 ± 0.4
4	3.6 ± 0.1

[a] Reaction conditions: [Mo] = 1mM, [Me_3NO] = 10 mM, in DMF at 27 °C. Data were analyzed by pseudo first-order kinetics, $d[Mo^{IV}]/dt = -k_{obs}[Mo^{IV}]$.

and destabilizes the O–O bond through the metal atom (push effect). However, rate constants in Table 4 apparently show no acceleration by the electronic effect. The rate constants decreases from 2.6 × 10^{-3} s^{-1} (for **1**) to 2.0 × 10^{-3} s^{-1} (for **2**), and from 5.7 × 10^{-3} s^{-1} (for **3**) to 3.6 × 10^{-3} s^{-1} (for **4**). Thus the O–N bond cleavage in coordinated Me_3NO is not involved in the rate-determining step.

In the 10-fold excess of Me_3NO, the above reaction was studied using ^{1}H NMR spectroscopy in the range 243–263 K. Table 5

Table 5. Temperature Dependence of the Rate Constants[38] for the Reaction of **1** and **2** with Me_3NO[a]

T, K	k_{obs}, s^{-1} **1**	**2**
300	2.6 (±0.5) × 10^{-3}	2.0 (±0.1) × 10^{-3}
263	5.9 (±0.9) × 10^{-5}	8.9 (±0.1) × 10^{-5}
253	3.8 (±0.4) × 10^{-5}	2.8 (±0.3) × 10^{-5}
243	2.9 (±0.2) × 10^{-5}	1.1 (±0.9) × 10^{-5}

[a] Reaction conditions: [Mo] = 1 mM, [Me_3NO] = 10 mM, in DMF at (300 K) and in DMF-d_7 (at 243, 253 and 263 K).

shows the rate constants analyzable by pseudo-first-order kinetics. Activation parameters could not be obtainable because the plot in the temperature dependence is not linear at 243–300 K ($\Delta S^{\ddagger} \sim -100$ J K^{-1} mol^{-1}, $\Delta H^{\ddagger} \sim 50$ kJ mol^{-1}) as shown in Figure 10. In the case of the more bulky complex **2**, the rate constants analyzed by pseudo-first-order kinetics (Table V) give a good least-squares fit of the k_{obs} values at 243–300 K to the Eyring equation[39] and give activation parameters ($\Delta S^{\ddagger}$ = −115 (±21) J K^{-1} mol^{-1}, $\Delta H^{\ddagger}$ = 54.4 (±5.6) kJ mol^{-1}) (Figure 10).

A large negative $\Delta S^{\ddagger}$ value suggests that the structure of transition state complex does not resemble the ground-state complex (= intermediate complex in Figure 9) that is the Me_3NO-coordinated intermediate of **1**. A possible transition state complex is, for example, a octahedrally coordinated *trans*-dioxo- or a trigonal prismatic coordinated *cis*-dioxomolybdenum(VI) complex or a trigonal prismatic monooxomolybdenum(IV) *N*-oxide adduct. If the transition state is stabilized by the DMF association, the activation entropy ($\Delta S^{\ddagger}$) will appear as a negative value. Thus, we concluded that the relatively large negative activation entropy from the solvation was observed kinetically.

If a *trans*-$(Mo^{VI}O_2)^{2+}$ species is formed at the transition state, it will be stabilized to a *cis*-$(Mo^{VI}O_2)^{2+}$ species. For such $(Mo^{VI}O_2)^{2+}$ species, mostly in octahedral ligand sets, cis geometry is observed exclusively.[40] From a theoretical analysis,[41] it is evident that Mo 4d orbitals play a dominant role in stabilizing the *cis*-$(Mo^{VI}O_2)^{2+}$ species.

Conclusion

The absence of μ-oxo dimerization is unusual for various reported molybdenum(IV) complexes, except for complexes with steric factors.[14,15] All the reported (μ-oxo)dimolybdenum(V)

(37) Yamaguchi, K.; Watanabe, Y.; Morishima, I. *J. Chem. Soc., Chem. Commun.* **1992**, 1709. Higuchi, T.; Uzu, S.; Hirobe, M. *J. Am. Chem. Soc.* **1990**, *112*, 7051.
(38) All errors in parentheses are random errors estimated at the 99% confidential level (2.5σ).
(39) $k_{obs} = (k_B T/h) \exp[\Delta S^{\ddagger}/R - \Delta H^{\ddagger}/RT]$. k_B = Boltzmann constant, h = Planck constant, R = gas constant, T = absolute temperature.
(40) Stiefel, E. I. *Prog. Inorg. Chem.* **1977**, *22*, 1.
(41) Tatsumi, K.; Hoffman, R. *Inorg. Chem.* **1980**, *19*, 2656.

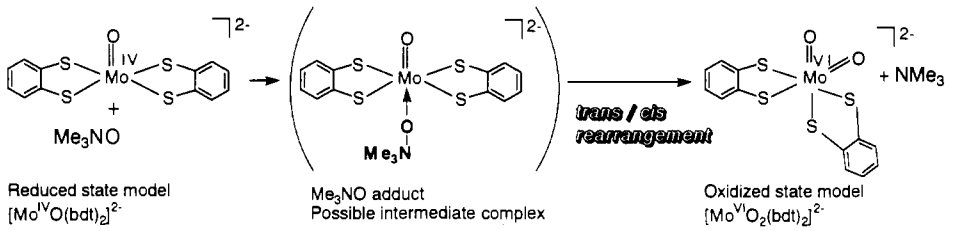

Figure 9. Proposed mechanism for the oxidation of $(NEt_4)_2[Mo^{IV}O(Ph_3Si\text{-}bdt)_2]$ (**1**) with Me_3NO.

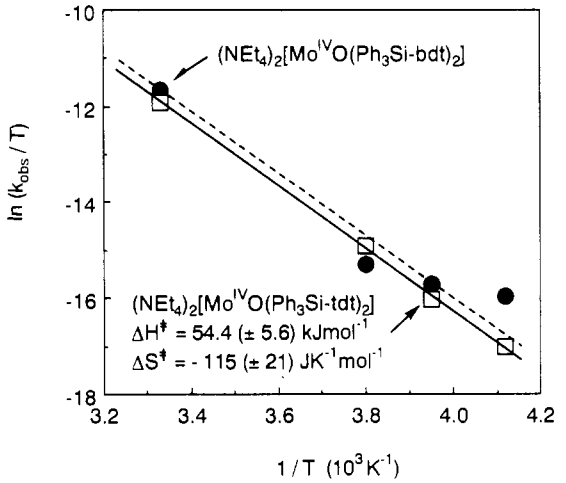

Figure 10. Eyring plots[39] for the oxidation reaction of $(NEt_4)_2[Mo^{IV}O(Ph_3Si\text{-}bdt)_2]$ (**1**) (- - -) and $(NEt_4)_2[Mo^{IV}O(Ph_3Si\text{-}tdt)_2]$ (**2**) (—) with Me_3NO. Reaction conditions: [Mo] = 1 mM, $[Me_3NO]$ = 10 mM, in DMF (at 300 K) and DMF-d_7 (at 243, 253 and 263 K).

complexes[42-44] have cis-configuration between terminal oxo and bridged oxo ligands. Therefore, a probable mechanism of the μ-oxo bridge formation involves an attack from one of the two oxo ligands of $(Mo^{VI}O_2)^{2+}$ to the vacant trans position $(Mo^{IV}O)^{2+}$ followed by trans–cis rearrangement among bdt and oxo ligands. Stabilization to the above *cis*-dioxo configuration finishes the reaction. This reaction pathway is essentially the same as proposed in Figure 9.

The inhibition of ligand isomerization is considered as one of the reasons of the lack of the formation of the (μ-oxo)-dimolybdenum(V) complex. The following result[45] indicates an electron transfer in the absence of isomerization. Thus, $[Mo^{VI}O_2(S_2CNEt_2)_2]$[46] reacts with $(NEt_4)_2[Mo^{IV}O(bdt)_2]$ (**3**) in acetonitrile to give a purple solution which apparently indicates the Mo(V) species. However, the expected mixed (μ-oxo)-dimolybdenum(V) species could not be detected upon the reaction and only formation of two species, $(NEt_4)[Mo^{V}O(bdt)_2]$ and $[(Mo^{V}O)_2(\mu\text{-}O)(S_2CNEt_2)_2]$,[43] ($S_2CNEt_2$ = *N*,*N*-diethyldithiocarbamato) was detected by ESR signals and absorption maximum, respectively. This indicates that the lack of the conproportionation reaction and of the ligand isomerization is caused by the stronger chelate binding of the bdt ligand as compared with the S_2CNEt_2 ligand. In the case of S_2CNEt_2, L-NS_2[10] (L-NS_2 = 2,6-bis(2,2-diphenyl-2-thiophenyl)pyridinate), and *t*-BuL-NS[15] complexes, weakly coordinating ligand atoms are considered to dissociate easily from the molybdenum ion. The ligand atoms—one of the sulfur atoms of the S_2CNEt_2 ligand and the nitrogen atoms of L-NS_2 and *t*-BuL-NS ligands—are not strongly chelating ones, which quite different from the dithiolene-like ditholato ligand, bdt.

In general, the observed unusual reactivity of monooxomolybdenum(IV) complexes reflects the difficulties of the dissociation and therefore of the isomerization caused by its strongly chelating ligands. Thus, (benzenedithiolato)monooxomolybdenum(IV) complexes react with a relatively strong oxo donor, such as Me_3NO, to form the corresponding dioxomolybdenum(VI) complexes, but the Mo(IV) complexes do not react with dioxomolybdenum(VI) complexes to form the (μ-oxo)dimolybdenum(V) species.

In the native enzymes, a sufficient dilution of molybdenum active sites in the protein has been proposed to cause the absence of the dimerization reaction.[12,13] Our results suggest that the coordination of a dithiolene ligand to the molybdenum ion controls electronically, not necessarily sterically, the reactivity of the active site to inhibit the stabilizing reactuion to form the (μ-oxo)-dimolybdenum(V) center of the enzymes even when the molybdenum site is exposed. Thus, Mo(IV) and Mo(VI) species are kept active for further reactions by the unique effect of dithiolene type ligands.

Supplementary Material Available: Tables of atomic positional and thermal parameters, bond distances, and bond angles (60 pages). Ordering information is given on any current masthead page.

(42) Dahlstrom, P. L.; Hyde, J. R.; Vella, P. A.; Zubieta, J. *Inorg. Chem.* **1982**, *21*, 927.
(43) Ricard; Estienne, J.; Karagiannidis, P.; Toledano, P.; Fischer, J.; Nitschler, A.; Weiss, R. *J. Coord. Chem.* **1974**, *3*, 277.
(44) Craig, J. A.; Harlan, E. W.; Snyder, B. S.; Whitener, M. A.; Holm, R. H. *Inorg. Chem.* **1989**, *28*, 2082.
(45) Ueyama, N.; Oku, H.; Kondo, M.; Nakamura, A. To be submitted for publication.
(46) Jowitt, R. N.; Mitchell, P. C. H. *J. Chem. Soc. A* **1969**, 2632. Chen, G. J.-J.; McDonald, J. W.; Newton, W. E. *Inorg. Chem.* **1976**, *15*, 2612.